19

SMALL-ANGLE X-RAY SCATTERING OF POLYMER SYSTEMS

Carlos A. Avila-Orta and Francisco J. Medellín-Rodríguez

19.1 INTRODUCTION

Semicrystalline thermoplastic polymers are widely used for a number of applications in food packaging, automotive parts, textiles, medical devices, etc., because of their excellent physical and chemical properties. In turn, these properties depend on the morphology developed by these crystalline systems. Unit cell, lamellar structure, and microstructure show different morphological features at different scales. In the nanoscale, the lamellar structure formed by alternating crystalline and amorphous layers predominates. Because of the length scale and the electron density difference between the crystalline and amorphous phases, this type of morphology is well suited to be studied by means of small-angle X-ray scattering (SAXS). This technique is useful to determine the crystalline and amorphous thicknesses and their distributions, as well as the crystal perfection. In this chapter, we describe the fundamentals of polymer morphology, one-dimensional data analysis in the reciprocal space as well as their possibilities in real space, and an application example.

19.2 POLYMER MORPHOLOGY

Polymers are considered macromolecular chains of high molecular weight formed by monomers bonded covalently. They can be obtained from natural sources or from synthetic processes through different polymerization routes [1]. A number of both natural and synthetic polymers are able to form regular arrangements, that is, crystalline entities, under either quiescent or deformed states. Cellulose and natural rubber are examples of natural polymers, while polyethylene (PE), isotactic polypropylene (iPP), and poly(ethylene terephthalate) (PET) are common synthetic polymers that can crystallize. The size, shape, and organization of the crystals depend on the chemical and molecular structure (stereoregularity, tacticity, molecular weight, chain flexibility) and crystallization conditions (quiescent, deformed, melt, solution). Although thermosets and rubbers can show crystalline behavior, thermoplastic polymers offer a wide range of possibilities, and so we focus our attention on this type of polymers.

Thermoplastic polymers are synthetic polymers that become plastic on heating and harden on cooling. PE, iPP, PET, and polyamides, among others, are typical examples of this type of polymers. Depending on the chemical and molecular structure and processing variables, they may or may not crystallize. Thermoplastic polymers that are able to crystallize have a significant amount of amorphous material, and therefore they are known as *semicrystalline thermoplastic polymers*.

The study of polymer morphology aims to elucidate the organization of crystalline domains [2]. Polymer morphology depends on the intrinsic properties of the polymer (chemical and molecular structure) as well as on the processing conditions (crystallization conditions, temperature, pressure, deformation, state). Besides, polymer morphology has a hierarchical structure. Polymer single crystals, spherulites, and shish kebabs are common polymer morphologies on the micrometer size, formed of lamellae on the nanometer scale (thickness), with unit cells in angstroms. These entities are the dimensional levels for the morphology of crystalline polymers.

Handbook of Polymer Synthesis, Characterization, and Processing, First Edition. Edited by Enrique Saldívar-Guerra and Eduardo Vivaldo-Lima.

19.2.1 Single Crystals, Spherulites, and Shish Kebabs

Polymer crystals can be obtained from either dilute solutions or amorphous states (glassy or molten) [2, 3]. Crystallization from dilute solutions usually gives polymer single crystals. Fischer, Keller, and Till reported the formation of polymer single crystals from dilute solutions [4]. On the other hand, three-dimensional polycrystalline structures named *spherulites* are usually obtained during polymer crystallization from the glassy or the molten state [5]. Bunn and Alcock and Keller found that polymers show this type of organization [6]. Finally, when the polymer solution or the amorphous state is under stress, long chains extend, serving as nuclei (shish), whereas smaller chains crystallize (kebab), usually in the form of a disk. Shish kebab structures were first observed by Mitsuhashi, Pennings, and Binsbergen [7].

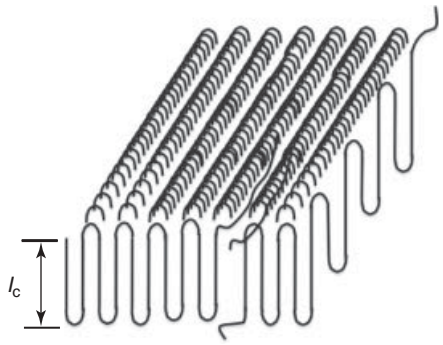

Figure 19.1 Scheme of unique crystal of folded chain for PE. *Source*: After Hoffman JD, Davis GT, Lauritzen JI. The rate of crystallization of linear polymers with chain folding. In: Hannay NB, editor. Treatise Solid State Chemistry, Volume 3, p 418, 508, 520 [8]. Copyright 1976 Plenum Press.

19.2.2 Lamellae

Polymer chains form regular arrangements while extended (extended chain crystals) or when they fold (chain-folded crystals or lamellae). The former is usually observed when crystallization conditions are near the thermodynamic conditions (near the equilibrium melting point), while the latter is governed by the kinetics at temperatures far away from the equilibrium conditions, where most industrial processes take place. In this case, polymer chains fold, forming thin lamellae with thicknesses ranging from 5 to 20 nm and widths in the range of micrometers. Keller inferred the existence of a chain-folded molecular conformation within polyethylene single crystals obtained from dilute solutions (4b). These thin crystals are known as *chain-folded crystals* when polymers are crystallized from dilute solutions, while they are named *chain-folded lamellae* or *lamellae* when they are crystallized from the amorphous (glassy or molten) state [8]. A scheme of a chain-folded crystal is shown in Figure 19.1, where the crystal thickness is denominated l_c.

The lamella is recognized as the component that imparts texture to most semicrystalline polymers. Besides, the surface regions of lamellae combine two different characteristics [2]. On one hand, there is evidence of order, and on the other, disorder. Both characteristics must be accommodated in the space of a crystalline unit. Therefore, the amorphous material alternates with lamellar crystals, resulting in the formation of lamellar structures (Fig. 19.2). Under quiescent conditions, lamellar crystals grow from a common radiating center forming spherulites, while for stressed melts cylindrical crystals alternate with amorphous material along an elongated nucleus to form shish kebab structures. Even when lamellar and spherulitic morphologies of crystallized polymers are different, lamellae should be inside spherulites, as is schematized in Figure 19.3 [8].

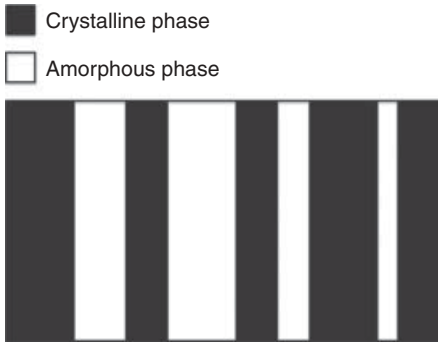

Figure 19.2 Scheme of lamellar structure.

19.2.3 Unit Cells

Chain-folded molecules ordered in a regular arrangement are three-dimensional crystals. A three-dimensional crystal is formed by a large number of smaller, hypothetical, three-dimensional crystals with sizes a, b, and c, named *unit cells*. Each unit cell contains a complete representation of the entire crystalline structure and gives the information needed to describe the whole arrangement. Depending on the conformation of the molecular chains and its own arrangement, any structure can be assigned to one of the six systems characterized by the ratios of the unit cell edges (a, b, and c) and their angles (α, β, and γ). The values of the unit cell constants are in general in the range of angstroms, which make them suitable to be studied by wide-angle X-ray scattering (WAXS). Semicrystalline polymers produce a mixed interference pattern, sharp and diffuse at the same time, when analyzed by WAXS [9]. This evidences the existence of a two-phase system, that is, a three-dimensional crystalline network with amorphous zones.

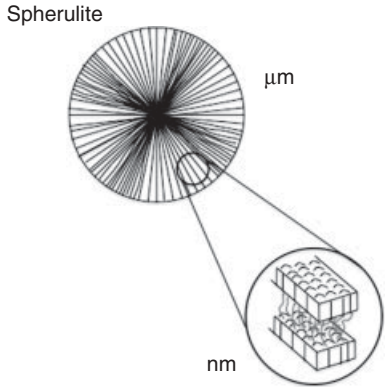

Figure 19.3 Spherulitic structure model. Note the growth direction and points of lamellar ramification, to fill void space with crystals in a uniform way. *Source*: After Hoffman JD, Davis GT, Lauritzen JI. The rate of crystallization of linear polymers with chain folding. In: Hannay NB, editor. Treatise Solid State Chemistry, Volume 3, p 418, 508, 520 [8]. Copyright 1976 Plenum Press.

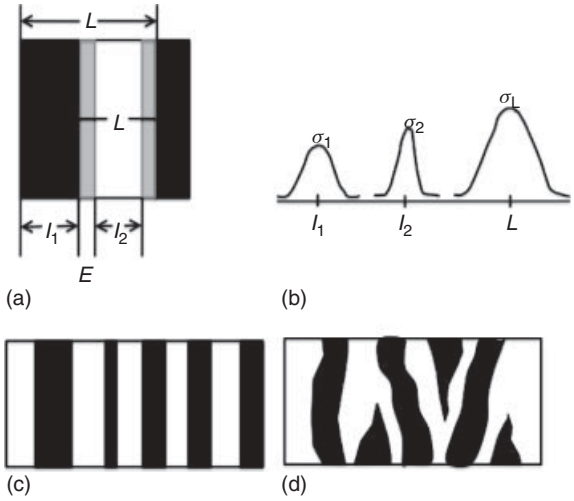

Figure 19.4 Physical representation of morphological parameters: (a) characteristic distances, (b) statistical features, (c) stacking size, and (d) interfaces planarity.

19.3 SMALL-ANGLE X-RAY SCATTERING

SAXS is a powerful tool to study the morphology of semicrystalline systems. The application of this technique is based on the electron density difference between the crystalline and amorphous phases (lamellar structure) in polymer systems. The crystalline (l_c) and amorphous (l_a) thicknesses can be obtained using this technique. Besides, the distance from one crystalline region to the next provides the size of a lamellar structure, also known as *the long period* (L). Other morphological features are the interface thickness (E), the thickness distribution (σ_c, σ_a, σ_L), the size of the lamellar stacking (t), and the dispersion capacity or invariant (Q). A schematic representation of some of these parameters is shown in Figure 19.4. Lamellar thicknesses l_c and l_a correspond to the average size of each phase. Since the technique cannot differentiate which thickness corresponds to the crystalline phase and which one to the amorphous phase, we denominate them as l_1 and l_2. The long period L is the distance between phases of the same type. Each of these thicknesses has a size distribution, typically Gaussian. The interface thickness E is the distance when the interface is not sharp, that is, the interface is finite. The lamellar stacking size can be finite or infinite.

19.3.1 Interaction of X-Rays with Matter

SAXS is determined by interference phenomena, where the waves are coherent and therefore their amplitudes can be added even if the emerging waves are not in phase as in the case of WAXS [10]. SAXS intensity is given by the absolute square of the resulting amplitude, which is obtained by summing all secondary waves. All amplitudes have the same magnitude and differ only in their phase ϕ, which depends on the electron position in space. The secondary scattering wave can be represented as $e^{i\phi}$, where ϕ is $2\pi/\lambda$ times the optical path δ and a reference point. Considering the number of electrons implied in the dispersion process, and the fact that an electron cannot be localized exactly, it becomes convenient to introduce the concept of electron density as described next.

19.3.2 Electron Density Function

Electron density function is defined as the number of electrons per unit volume and it is denoted as $\rho(r)$. Electron density function of a semicrystalline polymer consists of a series of alternating steps, positive ρ_1 and negative ρ_2, which represent phases, and fluctuate around an average value ρ_m. If, for example, an r vector is passed along the semicrystalline structure (Fig. 19.5), it can be seen that $\rho(r) = \rho_1$ if $\rho(r) > \rho_m$. On the other hand, $\rho(r) = \rho_2$ if $\rho(r) < \rho_m$, where ρ_1 is a high density region (crystalline) and ρ_2 is a low density region (amorphous).

19.3.3 Scattering Vector

Because of the inverse relation existing between the size of the scatterer and the distance of incidence of the source, experimental effects are observed in reciprocal space. Therefore, in order to obtain estimates in the reciprocal space, the geometry of a system with two dispersion centers which is impacted by X-ray beam is defined, determining a scattering vector in the reciprocal space, q.

In order to calculate the scattering vector q, it is necessary to calculate the phase ϕ. As previously mentioned,

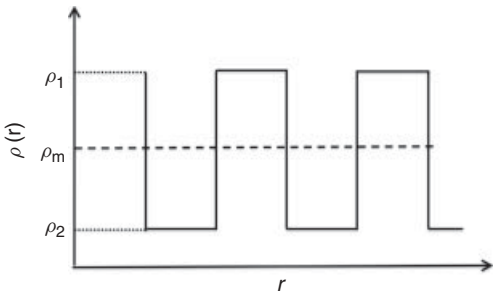

Figure 19.5 Schematic representation of the electron density function.

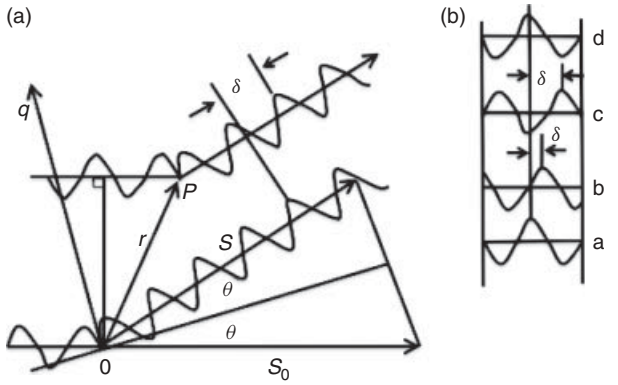

Figure 19.6 A (left). Geometry to obtain the scattering vector q. B (right). Wave enlargement: a, Reference wave; b, wave displaced $\delta(0 < \delta < 1)$; c, wave displaced $1\pi(\delta < 1/2)$; and d, wave displaced $2\pi(\delta = 1)$.

$\phi = 2\pi/\lambda \cdot \delta$. The distance from one dispersion center to another is called r, as shown in Figure 19.6A, where the unit vector s_0 has the direction of the incident beam and the unit vector s represents the vector of the dispersed wave. Bearing in mind this idea, $\delta = -r(s - s_0)$ can be defined, and therefore $\phi = -2\pi/\lambda \cdot r(s - s_0)$. The magnitude $(s - s_0) = 2 \cdot \sin\theta$, where θ is the angle of the scattering vector. A new q vector can be defined with direction $(s - s_0)$ and magnitude $4\pi/\lambda \cdot \sin\theta$ as

$$q = \frac{4\pi}{\lambda} \bullet \sin\theta \tag{19.1}$$

for which the phase $\phi = q \cdot r$. Then, the representation of a dispersed secondary wave in the complex form is e^{-iqr}. The vector product qr means that only the component of r in q is relevant for the phase, so that all the points in a plane perpendicular to q will have the same phase [10].

When the emergent waves of a scattering center in small angles are displaced in the range $(0 < \delta > 1, \delta \neq 1/2)$ with respect to a reference wave, a dispersion phenomenon occurs (Fig. 19.6B, case b). If the emergent wave is displaced by $\delta = 1/2$, then widths of the waves cancel out and dispersion does not take place (Fig. 19.6B, case c). These two cases do not produce diffraction (WAXS) since the condition for the diffraction phenomenon to take place is that the waves must be in phase, thas is, $\delta = 1$, as illustrated in case (d) of Figure 19.6B.

Additionally, this condition is also necessary in order to produce the phenomenon of scattering. In short, WAXS and SAXS techniques depend on the value of δ. In the range $(0 < \delta \leq 1, \delta \neq 1/2)$ this condition is fulfilled, so that the scattering phenomenon (SAXS) is produced; the diffraction phenomenon (WAXS) is produced if and only if $\delta = 1$.

19.3.4 Scattering Intensity

Assuming a unique dispersion process and the applicability of the theory of kinematic dispersion, the intensity of dispersion $I(q)$ is given by

$$I(q) = \Im\left[\Delta p^{*2}(r)\right] \tag{19.2}$$

where $\Delta\rho(r)$ is the difference between the local and the average electronic densities $(\rho(r) - \rho_m)$, $\Im$ represents the three-dimensional Fourier transform, and the term *2 indicates an autoconvolution or autocorrelation [11]. Then Equation 19.2 can be rewritten as

$$I(q) = \int_v \Delta p^{*2}(r) \bullet e^{-iqr} dV \tag{19.3}$$

In Equation 19.3, it is observed that the real space (r) and the reciprocal space (q) are connected by the phase qr, and naturally q will diminish when r increases, and vice versa, with the same factor. In this way, large particles will give a concentrated scattering pattern in small angles. Especially with particles or heterogeneities of colloidal dimensions, and with a wavelength of 1.5 Å, the dispersion pattern is limited to 1° or 2° of the scattering angle. This is the typical domain of SAXS.

In SAXS, two restrictions are generally present which simplify the analysis of scattering:

1. The system is statistically isotropic. Because of this restriction, the distribution $\rho^{*2}(r)$ depends only on the magnitude of the distance r. Additionally, the phase factor e^{-iqr} can be replaced by its average taken in all directions and it is expressed as [12]

$$\left\langle e^{-iqr} \right\rangle = \frac{\sin(qr)}{qr} \tag{19.4}$$

Then Equation 19.3 can be written as

$$I(q) = \int_V 4\pi r^2 \Delta p^{*2}(r) \bullet \frac{\sin(qr)}{qr} dr \tag{19.5}$$

2. Long-range order does not exist [12]. This means that correlation between two widely separated points does not exist. In accordance with the above, at large values of r, the electron densities would be independent, and they could be replaced by the average value ρ_m. In this way, the structure is represented by the finite region where $\rho^{*2}(r)$ deviates from the mean value, and therefore values of r widely separated do not provide information.

19.4 ANALYSIS IN RECIPROCAL SPACE

An experimental intensity curve as a function of the scattering vector is produced in SAXS. From the isotropic patterns of a melt-crystallized polymer, a slice is taken and, when projected in the plane $I(q)$ against q, it shows a scattering maximum with a wide statistical distribution. The evaluation of structural parameters from the intensity curve requires the whole scattering curve. Nonetheless, the lower and upper ends of the curve cannot be determined because of the nature of the scattering process. Therefore, mathematical approximations are used to access both ends of the curve. According to the characteristics of the dispersion function measured experimentally, the intensity curve is divided into three parts, which are described in the following sections.

19.4.1 Scattering Intensity when $q \to 0$

As previously mentioned, it is not possible to obtain the experimental intensity data for q values near zero; therefore, it is desirable to extrapolate the obtained data down to $q = 0$. This can be done by means of models or using arbitrary extrapolations (straight lines, polynomials, etc.). When using models in this region, it is possible to obtain information about the average radius of gyration and the radius for a spherical domain, as well as the size of the inhomogeneities [13]. For a system of isolated domains at high dilutions, Guinier and Fournet (13a) proposed

$$\underset{q\to 0}{I(q)} = K_{\mathrm{G}} \mathrm{e}^{\left[\left(-R^2/3\right)q^2\right]} \tag{19.6}$$

where K_{G} is a constant and R is the average radius of gyration, given by $R = (3/5)^{1/2} R_{\mathrm{d}}$ for a spherical domain of radius R_{d}. Then, by means of a plot of $\ln[I(q)]$ versus q^2, it will be possible to obtain the parameters K_{G} and R.

Debye et al. (13b) developed a model for random scatterers, which is given by the expression

$$\underset{q\to 0}{I(q)} = \frac{A}{\left(1 + \varepsilon^2 q^2\right)^2} \tag{19.7}$$

where A is a constant and ε is the length of the inhomogeneity. By means of a plot of $1/I(q)^{1/2}$ versus q^2, it will then be possible to obtain the parameters A and ε. Equations 19.6 and 19.7 can be used for extrapolating the intensity $I(q)$ at $q = 0$ if there is enough data near $q = 0$.

19.4.2 Scattering Intensity at Intermediate Angles

Most semicrystalline polymers give rise to SAXS patterns that are characterized by one or more maxima in the dispersion curve. These patterns have been interpreted in terms of a simple model of crystalline and amorphous regions that alternate regularly [14]. The angular position of the maximum of diffraction (Bragg's law) and its correction for time of collection (the Lorentz factor) can be interpreted to provide the average structural period (periodicity L) of the polymer. In the following paragraphs, the possibilities for this region are given.

19.4.2.1 Bragg's Law In the analysis of semicrystalline polymers, in a first approach, it can be assumed that L is associated with the distance between the lamellar planes. These distances can be related through the Bragg's law with the diffracted waves that are in phase and are reinforced in certain directions (angles) [15]. This analysis give values that qualitatively coincide with the structure observed by means of electron microscopy and with sizes of crystals indicated by means of WAXS [16]. The periodicity L is related to the vector q in the maximum of dispersion according to [17]

$$L = \frac{2\pi}{q_{\max}} \tag{19.8}$$

However, in most cases the structural sizes inferred from this treatment do not agree with the structures observed by means of electron microscopy [18]. For instance, polymers crystallized from the molten state rarely have orders of multiple dispersion (as required by diffraction) and, moreover, they present a wide first-order peak as shown in Figure 19.7 [19]. Then, when applying the Bragg's law, the obtained period will be distorted considerably from the average period of the structure [14]. This discrepancy of values can decrease, but not vanish, when applying the Lorentz factor to the curve of observed intensity.

19.4.2.2 The Lorentz Factor L_0 The factors that rule the diffraction intensity $I(hkl)$ are the structure factor for atomic dimensions $F(hkl)$, the polarization factor P, the Lorentz factor L_0, and the multiplicity factor j. However, in studies of SAXS, all factors except the Lorentz factor can be omitted [9].

In diffraction, the Lorentz factor depends basically on the reflection time, that is, the time during which a family of planes reflects X-rays under certain experimental

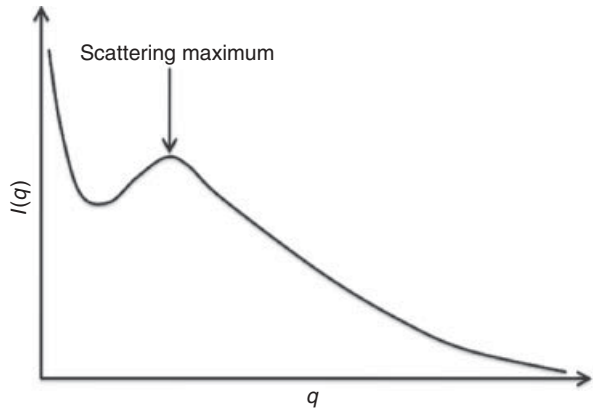

Figure 19.7 Scheme of a typical SAXS curve of $I(q)$ versus q of a semicrystalline polymer.

conditions. The time of reflection originates partly because of the lack of parallelism and monochromaticity of the incident beam [9].

In SAXS studies of a real sample, all the lamellar layers or stacks are oriented at random with respect to the incident beam; therefore the intensity function $I(q)_{\text{obs}}$ which corresponds to the measured intensity shows spherical symmetry [20]. However, when using theoretical one-dimensional models (where the lateral width of the lamellae is much greater than the periodicity), the dispersion intensity is calculated assuming that the lamellar stacks are correctly oriented (perpendicular) with respect to the incident beam [21]. This implies that the observed intensity (with spherical symmetry) should be corrected to a perpendicular intensity to the lamellar stacks. Because of this, the Lorentz factor that is described for lamellar systems is also used.

The nature of the inhomogeneities of semicrystalline polymers can be expressed for spherically symmetric dispersion by means of a structure factor $F(q)$. For X-ray dispersion, this can be represented as

$$I_{\text{obs}}(q) = \overline{|F(q)|^2 \bullet L_0} \tag{19.9}$$

where L_0 plays a similar role as the Lorentz factor in classical X-ray crystallography.

The form of L_0 in Equation 19.9 depends on the experimental conditions used, the form of the scatterers, and the searched parameters. For instance, it is proportional to q^{-2} for point collimation and to q^{-1} when collimation is made through a grid [9]. On the other side, independent of the collimation system utilized, L_0 is proportional to q^{-1} when the section of a cylindrical particle is determined, while it is proportional to q^{-2} when the thickness of a laminar particle is determined [22].

On the other hand, it is well known that the ideal intensity generated by the structure with a factor $F(q)$ is given by the absolute square of this factor [9, 10], that is,

$$I_{\text{id}}(q) = |F(q)|^2 \tag{19.10}$$

Considering that the factor L_0 for point collimation and for laminar particles (one-dimensional model) is q^{-2}, substituting Equation 19.10 in Equation 19.9 and rearranging gives

$$I_{\text{id}}(q) = I_{\text{obs}}(q) \bullet q^2 \tag{19.11}$$

Equation 19.11 means that the observed intensity must be multiplied by a factor q^2 to obtain a better estimation of the periodicity in lamellar systems of semicrystalline polymers. The factor q^2 is related to the change from the scatterers oriented at random to dispersers perfectly aligned (Fig. 19.8). This correction is implied, for instance, in the use of models of one-dimensional stacking [19]. As $I_{\text{id}}(q)$ has been obtained from a one-dimensional model, it can be written as $I_1(q)$ [19].

In summary, the purpose of the Lorentz factor is to allow the comparison of an anisotropic intensity (in reciprocal space) calculated from a model with the obtained experimental intensities of samples whose symmetry (due to static or time-averaged disorientations) is generally different from that of the model [22]. It also takes into account the fact that only the intensity in reciprocal space that intersects the Ewald sphere can be observed experimentally [23]. Also, the time-averaged orientations may be related to the collimator type and the particle shape. This region in general has a well-defined shape, therefore only polynomial adjustments are made if necessary in order to avoid experimental noise.

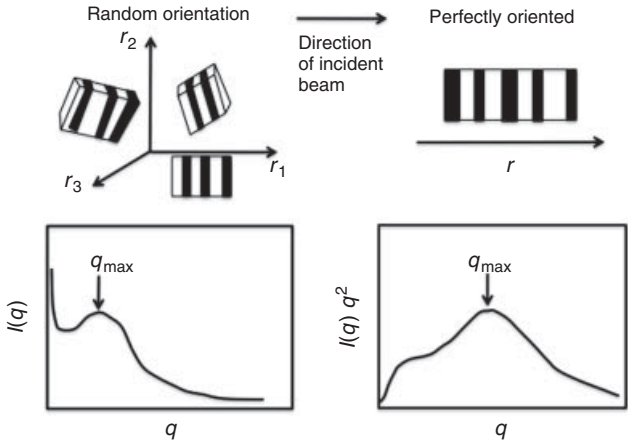

Figure 19.8 Rearranging of scatterers from random orientation to perfectly oriented with respect to the incident beam.

19.4.3 Scattering Intensity when $q \to \infty$

The third region of the scattering intensity curve is known as *Porod's region* and it contains information on the phase limits. This region is located at large scattering angles and after the first-order maximum for semicrystalline polymers. By analyzing this region, it is possible to determine the interface thickness between the phases and whether the polymer has fluctuations of electronic density inside the phases [11]. The possible types of calculation in this region are described below.

19.4.3.1 Ideal System without Interface (Porod's Law) According to the Equation 19.2, the intensity of dispersion for an ideal structure will be the Fourier transform of the autoconvolution of the difference between the local and the average electronic densities, that is,

$$I_{\mathrm{id}}(q) = \Im\left[\Delta\rho_{\mathrm{id}}^{*2}(r)\right] \tag{19.12}$$

Porod predicted that, for an ideal lamellar system of two phases (Fig. 19.5) in which neither fluctuations of density within phases nor interfacial thickness of finite wide are present, the intensity of dispersion diminishes proportionally to the reciprocal of the fourth power of q, which is mathematically expressed as

$$I_{\underset{q\to\infty}{\mathrm{id}}}(q) = \frac{K_{\mathrm{p}}}{q^4} \tag{19.13}$$

where K_{p} is the Porod constant, and Equation 19.13 is called *Porod's law* [24]. The determination of K_{p} is important because of the fact that it is related to certain structural parameters of the system, that is,

$$K_{\mathrm{p}} = \left(\frac{S}{V}\right)\left(\frac{Q}{8\pi^3\phi_1\phi_2}\right) = \frac{Q}{2\pi^3 l_{\mathrm{p}}} \tag{19.14}$$

where Q is known as the *three-dimensional Porod invariant* and it is given by

$$Q = \int_0^\infty q^2 I(q)\mathrm{d}q = V\phi_1\phi_2\left(\rho_1 - \rho_2\right)^2 \tag{19.15}$$

S/V is the area of the interface per unit volume, ϕ_1 and ϕ_2 are the volume fractions of the phases ρ_1 and ρ_2, respectively, and l_{p} is the longitude of the Porod inhomogeneity, a parameter that serves as a measure of the average size of the phases in all the directions of densities ρ_1 and ρ_2.

If the interfaces of the lamellae are totally flat and the lateral dimensions are very large compared to the thickness of the lamellae, the total interfacial area S_0/V is given by

$$\frac{S_0}{V} = \frac{2}{L} \tag{19.16}$$

where the parameter L is called *periodicity* or *long period*. If the interfaces are not flat, the obtained interfacial area S obtained from l_{p} is larger than S_0 obtained from L. Therefore, the relationship

$$\frac{S}{S_0} = \frac{2\phi_1\phi_2 L}{l_{\mathrm{p}}} = \frac{2l_1 l_2}{L l_{\mathrm{p}}} \tag{19.17}$$

is a measure of the planarity of the interfaces.

19.4.3.2 System with Finite Interface (Negative Deviations of Porod's Law) Tsvaskin and Blundell were the first to consider that polymers show a transition area between the crystalline and amorphous phases of length E, which was taken into account in theoretical models [21, 25]. This finite thickness (E) of the amorphous–crystalline interface causes semicrystalline polymers to exhibit deviations from the ideality dictated by the Porod's law [11]. This thickness can be represented through a smoothing function in real space, that is, $h(r)$. According to Ruland (1971), this function convolutes with the Fourier transform of the autoconvolution of the difference between the local and the average electronic densities to reproduce the gradient profile of the interfacial density of a structure with finite thickness, that is,

$$\Delta\rho_{\mathrm{E}}(r) = \Delta\rho_{\mathrm{id}}(r) * h(r) \tag{19.18}$$

where $\Delta\rho_{\mathrm{E}}(r)$ is the difference between the local and the average electronic densities for a structure with finite thickness [11]. The Fourier transform of a convolution product in real space is equivalent to the product of those Fourier transforms in reciprocal space. From Equations 19.2 and 19.18, one can obtain the scattering intensity for this particular case as

$$I_{\mathrm{E}}(q) = \Im\left[\Delta\rho_{\mathrm{id}}^{*2}(r)\right]\Im\left[h^{*2}(r)\right] \tag{19.19}$$

or

$$I_{\mathrm{E}}(q) = I_{\mathrm{id}}(q) \bullet H^2(q) \tag{19.20}$$

$I_{\mathrm{E}}(q)$ is the intensity of dispersion for a structure with finite thickness, and $H^2(q)$ is the Fourier transform of $h^{*2}(r)$ in the reciprocal space. Because the width of the function $h(r)$ should be small compared to the average regions of constant density (for a two-phase system), the width of the function $H(q)$ will be considerably larger than that of the intensity. In this way, the intensity of dispersion is affected essentially only at large q values, that is, in the Porod's region. As a consequence, and using Equation 19.13, the result is

$$I_{\mathrm{E}}(q) = \frac{K_{\mathrm{p}}}{q^4} \bullet H^2(q) \tag{19.21}$$

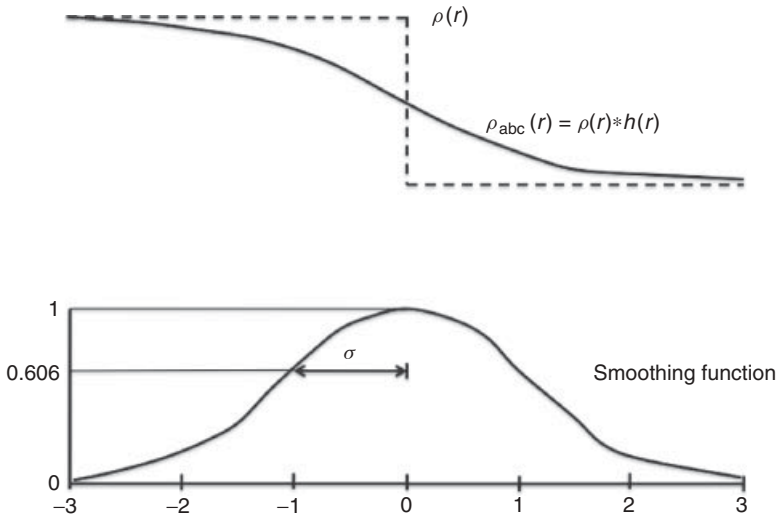

Figure 19.9 Sigmoidal model of gradient of interface. *Source*: Reproduced with permission from Koberstein JT, Morra B, Stein RS. J Appl Crystallogr 1980;13:34 [27]. Copyright 1980 IUCr (International Union of Crystallography) (http://dx.doi.org/10.1107/S0021889880011478).

where the shape of the smoothing function is defined by the geometric model used for the interfacial gradient.

The sigmoidal model for the interfacial gradient was introduced by Ruland and consists of a Gauss-type change of the electron density, as shown in Figure 19.9 [11]. The smoothing function is then Gaussian and $H(q)$ is given by

$$H(q) = \mathrm{e}^{\left[-\frac{(\sigma^2 q^2)}{2}\right]} \tag{19.22}$$

where σ is the standard deviation of the smoothing Gaussian function related to the finite thickness [26]. Inserting Equation 19.22 into Equation 19.21, the resulting scattering intensity is given by

$$I_{\mathrm{E}}(q) = \frac{K_{\mathrm{p}}}{q^4} \bullet \mathrm{e}^{\left[-\left(\sigma^2 q^2\right)\right]} \tag{19.23}$$

The value of σ can be defined using the curve of $\ln[I_{\mathrm{E}}(q)q^4]$ versus q^2. This represents a linear relationship with negative slope where Porod's law is fulfilled (negative deviation of Porod's law). By expanding the exponential function, the intensity can be approximately calculated by

$$I_{\mathrm{E}}(q) = \frac{K_{\mathrm{p}}}{q^4} \bullet \mathrm{e}^{\left[1-\left(\sigma^2 q^2\right)\right]} \tag{19.24}$$

Therefore, in a curve of $I_{\mathrm{E}}(q)q^4$ versus q^2, a linear region with negative slope should be located where Porod's law is fulfilled. The slope obtained by Equations 19.23 and 19.24 is related to the structural parameters through the expression [11]

$$\text{Slope} = -\frac{Q\sigma^2 q^2}{2\pi^3 l_{\mathrm{p}}} \tag{19.25}$$

The straight line extrapolated to $q = 0$ intersects the $I_{\mathrm{E}}(q)q^4$ axis at $Q/(2\pi^3 l_{\mathrm{p}})$, which enables the calculation of the value of K_{p}. On the other hand, σ and E are related by [26]

$$E = (2\pi)^{1/2}\sigma \tag{19.26}$$

Another model for the electron density gradient was proposed by Blundell and analyzed by Vonk; it consists of a linear density change in the interface [21, 28]. In this model, called the *geometric linear model*, the smoothing function is of rectangular type (Fig. 19.10) and its Fourier transform is given by

$$H(q) = \frac{\sin(Eq)}{Eq} \tag{19.27}$$

where E is the interfacial thickness. The dispersion of intensity is given by

$$I_{\mathrm{E}}(q) = \frac{K_{\mathrm{p}}}{q^4} \bullet \frac{\sin^2(Eq)}{(Eq)^2} \tag{19.28}$$

A drawback of this equation is that it cannot be treated in graphical form. However, by expanding the sine function in a power series truncated after the second term, a more manageable form can be obtained as follows:

$$I_{\mathrm{E}}(q) = \frac{K_{\mathrm{p}}}{q^4} \bullet \left[1 - \frac{E^2 q^2}{3}\right] \tag{19.29}$$

From this, by plotting $I_{\mathrm{E}}(q)q^4$ versus q^2, a linear region of negative slope can be located where the Porod's law is fulfilled if the thickness is finite.

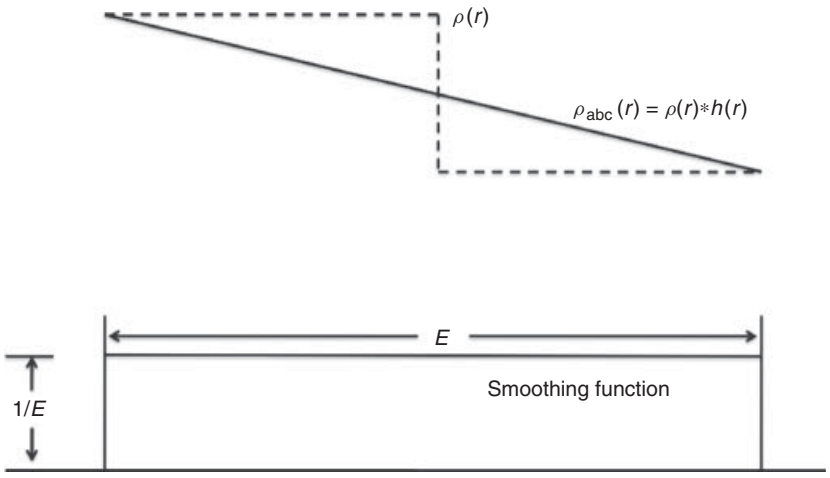

Figure 19.10 Linear model of the interface gradient. *Source*: Reproduced with permission from Koberstein JT, Morra B, Stein RS. J Appl Crystallogr 1980;13:34 [27]. Copyright 1980 IUCr (International Union of Crystallography) (http://dx.doi.org/10.1107/S0021889880011478).

19.4.3.3 System with Fluctuations within the Phases (Positive Deviations of Porod's law) Besides presenting interfacial thicknesses of finite width, semicrystalline polymers generally have electron density fluctuations inside the phases denoted FL [11]. Such electron density fluctuations are associated with thermal and density fluctuations. These fluctuations cause a global increment in the scattering intensity, which is denoted I_{FL}. This effect is different from that exhibited at high values of the dispersion vector where it is also observed that the intensity curve grows because of the beginning of the WAXS region [27]. The increment in the scattering intensity caused by the presence of fluctuations inside the phases, which is limited by the beginning of the WAXS region, is known as the *background intensity* $I_B(q)$ [29].

With the aim of determining the value of $I_B(q)$, Vonk proposed that the function $I_B(q)$ can be expanded in a power series truncated at the first or second term, according to

$$I_B(q) = I_{FL} + b_1 q^n \tag{19.30}$$

where b_1 is a constant, n is an integer, and I_{FL} is the value of the intensity extrapolated to $q = 0$ [28].

According to Ruland, $I_B(q)$ can also be approximated by an exponential function, which is expressed as

$$I_B(q) = I_{FL} \cdot e^{b_2 q^2} \tag{19.31}$$

where b_2 is a constant and I_{FL} is the value of the intensity extrapolated to $q = 0$ [30].

If the background intensity $I_B(q)$ is added to the intensity produced by systems with interfacial thickness, $I_E(q)$, the following expression can be obtained:

$$I_{EXP}(q) = I_{id}(q) \cdot H^2(q) + I_B(q) \tag{19.32}$$

which is the fundamental equation that describes the experimental intensity in semicrystalline polymers [11]. As a good approximation, it is possible to consider $I_B(q)$ a constant and equal to I_{FL}. In this case, it is possible to evaluate $I_B(q)$ from the positive slope of a plot of $I_{EXP}(q)$ versus q^4 (positive deviation of Porod's law) if it is assumed that $H^2(q)$ is constant as a first approximation [11, 31].

Equation 19.32 can be modified to outline the intensity of an ideal system, $I_{id}(q)$:

$$I_{id}(q) = \frac{I_{EXP}(q) - I_B(q)}{H^2(q)} \tag{19.33}$$

where $I_B(q)$ can be a constant, an exponential, or a power series, $H^2(q)$ can be unity ($E = 0$; $\sigma = 0$), geometric sigmoidal, sigmoidal expanded, linear geometric, or linear expanded. The ideal intensity curve can be produced by different ways. Siemann and Ruland proposed a method of trial and error adjusting the parameters K_P, σ, and I_B; Medellin and Avila applied a technique of numerical parameter fitting using the quasi-Newton method for PET [26, 32].

19.5 ANALYSIS IN REAL SPACE

19.5.1 Correlation Function, $\gamma(r)$

Debye and Bueche introduced the correlation function when studying porous solids [33]. The correlation function is based on the fluctuations of local densities with respect to an average value ($\eta_1 = [\rho_1(r) - \rho_m]$) where $\rho_1(r)$ is a local value and ρ_m is the average value. Since this function depends only on density fluctuations, it can be used for semicrystalline polymers where strong density

deviations exist [20]. The correlation function can be seen in the following way: consider two neighboring points in the system, located at a distance r [33, 34]. Take the product of both fluctuations $\eta_1 = \rho_1(r) - \rho_m$ and $\eta_2 = \rho_2(r) - \rho_m$, the first taken at point 1 and the second taken at point 2. Move points 1 and 2 through the material, maintaining a fixed distance r. If a large number of values of the product $\eta_1\eta_2$ are obtained, then the average value of this product indicated by $\langle\eta_1\eta_2\rangle_m$ can be found. According to this discussion, this product depends on the distance r. If $r = 0$ then $\eta_2(0) = \eta_1(0)$, and therefore, the previous product is given by $\langle\eta_1\eta_2\rangle_m = \eta_2$. For large r values, the product will be zero because the fluctuations will vary independently. In general, $\langle\eta_1\eta_2\rangle_m$ will be a function of the distance r, starting at η^2 for $r = 0$ and decaying to zero when increasing the value of r. Then, it can be concluded that the average extension of the heterogeneities is given by the relationship $\langle\eta_1\eta_2\rangle_m/\eta^2$, which is known as the *correlation function* and does not have physical dimensions; that is, it is a dimensionless number that varies with the distance and indicates the average extension of the heterogeneities.

$$\gamma(r) = \frac{\langle\eta_1\eta_2\rangle_m}{\eta^2} \tag{19.34}$$

19.5.1.1 Experimental Correlation Function γ(r) Following a similar process, Vonk and Kortleve introduced the correlation function for semicrystalline polymers, but in a single dimension (Fig. 19.8) [20]. If the cosine Fourier transform of the correlation function is obtained, then

$$\gamma_1(r) = \frac{\int_0^\infty I_1(q)\cos(qr)\mathrm{d}q}{\int_0^\infty I_1(q)\cos(0)\mathrm{d}q} \tag{19.35}$$

where $\cos 0 = 1$. Replacing the value of $I_1(q)$ by its equivalent in $I(q)$ (Eq. 19.11), the function $\gamma_1(r)$ becomes

$$\gamma_1(r) = \frac{\int_0^\infty q^2 I(q)\cos(qr)\mathrm{d}q}{\int_0^\infty q^2 I(q)\mathrm{d}q} \tag{19.36}$$

where $\gamma_1(r)$ is the one-dimensional correlation function and the denominator is the invariant Q (Eq. 19.15). In this way, the correlation function $\gamma_1(r)$ is normalized by the invariant Q, having an initial value of 1. This function shows a series of maxima and minima of diminishing height, which finally become zero at large values of r. This behavior suggests a periodicity in the structure; the position of the first maximum corresponds to the average value of the distance of periodicity, in other words, the long period L.

In many cases, $\gamma(r)$ depends only on the distance r and not on the direction in the space of this vector; therefore, integration over all directions can be done [33]. In the cases of polyethylene and polytetramethylene, Fulcher *et al*. used the following relation [35]:

$$\gamma_3(r) = \frac{\int_0^\infty q^2 I(q)\left(\frac{\sin(qr)}{qr}\right)\mathrm{d}q}{\int_0^\infty q^2 I(q)\mathrm{d}q} \tag{19.37}$$

where γ_3(r) is the three-dimensional correlation function which depends only on the magnitude of the distance r. The form of this function is similar to the one shown for the function $\gamma_1(r)$, but the information that they provide is not the same.

From the previous paragraph, it follows that r is a vector perpendicular to the layers of the crystalline and amorphous regions for $\gamma_1(r)$ or in any direction for $\gamma_3(r)$. In a medium in which γ depends originally on r and not on their directions, under stress, γ will begin to depend also on the direction of r [33]. In this case, the scattering intensity does not have a symmetry center around the direction of the primary beam. The same thing happens if the heterogeneities are aligned along a common axis. Therefore, when carrying out the analysis of the morphology of lamellar systems, it is advisable to meditate in an appropriate way the required information for the system under study.

19.5.1.2 Form and Properties of the One-Dimensional Correlation Function A periodic structure with a given electron density function $\rho(r)$ can be described by means of the long period L, the crystalline thickness l_c, and the difference of electronic densities $\Delta\eta = \rho_c - \rho_a$. The effect of different lamellar systems on the form and properties of the one-dimensional correlation function was discussed by Strobl and Schneider [36]. Next, systems of two phases and their impact are presented, giving the form and characteristics of the correlation function $\gamma_1(r)$, in accordance with these authors.

19.5.1.3 Ideal Lamellar System of Two Phases In an ideal lamellar system, the interface thickness and the density fluctuations within the phases are negligible, and the structure can be described by the long period L, the crystalline thickness l_c, and the electron density distribution, as shown in Figure 19.11a with their corresponding function $\gamma_1(r)$ for the irradiated volume. In this case, the form of the function $\gamma_1(r)$ consists of a series of autocorrelation triangles which show a periodicity L. The autocorrelation triangle centered in the origin has a number of important characteristics. The value of $\gamma_1(r)$ at $r = 0$ is the invariant Q. The line between the triangles is known as the *baseline*. Its negative coordinate is given by

$$-A = -\phi_c^2\left(\rho_c - \rho_a\right)^2 \tag{19.38}$$

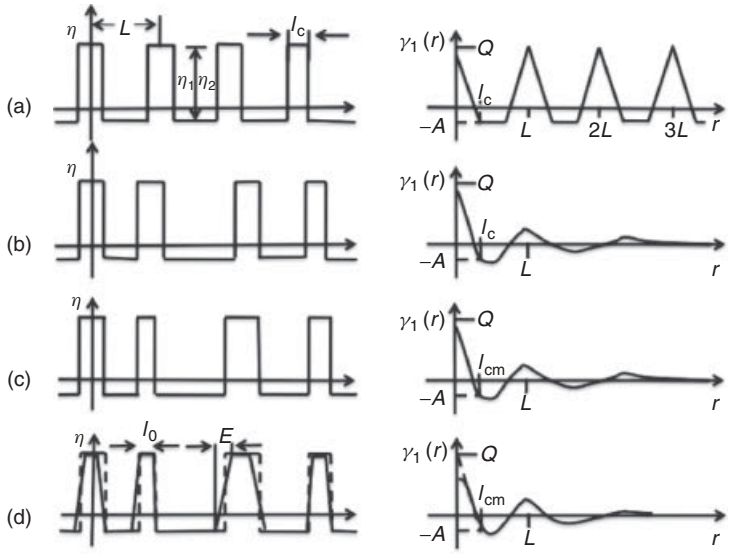

Figure 19.11 Representation of a system of two phases and their impact in the function $\gamma_1(r)$. (a) Periodic system of two phases, (b) effect of variations in the period L, (c) effect of additional thickness fluctuations, (d) effect of the introduction of diffuse frontiers (interface thickness). *Source*: Reproduced with permission from Strobl GR, Schneider M. J Polym Sci Polym Phys Ed 1980;18:1343 [36]. Copyright 1980 Wiley Periodicals, Inc.

Therefore, the height of the triangle becomes

$$Q + A = \phi_c \left(\rho_c - \rho_a\right)^2 \tag{19.39}$$

Hence, the slope $d[\gamma_1(r)/dr] = -S_0/2(\rho_c - \rho_a)^2$ (Eq. 19.17)The first intersection of the function $\gamma_1(r)$ with the axis $r[\gamma_1(r) = 0]$ occurs at

$$r_0 = I_c \left(I - \phi_c\right) \tag{19.40}$$

The function $\gamma_1(r)$ intersects the baseline at $r_1 = l_c$.

19.5.1.4 Ideal Lamellar System of Two Phases with Variation in the Interlamellar Space Because the autocorrelation part remains the same, in this case the only consequence is an enlargement in the width of the peak due to the closer correlations (Fig. 19.11b). Additionally, the position of the maximum provides the periodicity, which denotes the most probable spacing.

19.5.1.5 Ideal Lamellar System of Two Phases with Variation in the Interlamellar Space and Thickness If ϕ_c and S_0 are kept constant, then the invariant Q, the slope $d[\gamma_1(r)/dr]$, and the baseline A are not affected. Nonetheless, a change occurs near the base of the triangle where $\gamma_1(r)$ becomes curved (Fig. 19.11c). The straight section of $\gamma_1(r)$ will intersect the axis r at

$$r_0 = \frac{-Q}{d\gamma/dr} = \left(1 - \phi_c\right) \frac{\phi_c}{S_0/2} = \left(1 - \phi_c\right) I_{cm} \tag{19.41}$$

and the baseline at

$$r_1 = \frac{Q + A}{d\gamma_1/dr} = \frac{\phi_c}{S_0/2} = l_{cm} \tag{19.42}$$

In these equations, l_{cm} denotes the average (in number) lamellar thickness and can be defined as

$$l_{cm} = \phi_c L \tag{19.43}$$

19.5.1.6 Ideal Lamellar System of Two Phases with Variation in the Interlamellar Space, in the Lamellar Thickness, and in the Presence of Interface Thickness The presence of a transition zone changes the shape of the correlation function near the origin (Fig. 19.11d). However, the original straight line does not change. This happens because the thickness of the transition area E is smaller than the average thickness for all the lamellae, l_{c0}. In this case, the original straight line is located between $r = E$ and $r = l_{c0,min}$, where $l_{c0,min}$ denotes the average thickness of the thinnest lamellae of the system.

It is possible to directly derive the parameters of this system. The extrapolation of the linear section to $r = 0$ corresponds to its invariant Q, which is generally larger than the fluctuation of the square average electron density $\gamma_1(0)$ of the real structure. All the basic

structural parameters of this type of system are obtained by means of

$$\phi_c = \frac{A}{A+Q} \tag{19.44}$$

$$l_{cm} = r_1 \tag{19.45}$$

$$l_{cm} = \frac{r_0}{1-\phi_c} \tag{19.46}$$

$$S_0 = \frac{2\phi_c}{l_{cm}} \tag{19.47}$$

$$(\eta_c - \eta_a)^2 = \frac{Q}{\phi_c(1-\phi_c)} \tag{19.48}$$

In another method of graphic analysis, proposed by Vonk, the average thickness of the lamellae, l_{cm}, is evaluated from the following equation:

$$l_{cm} = Qr_1 + \frac{E}{3} \bullet \frac{\phi_c}{1-\phi_c} \tag{19.49}$$

In this way, the analysis has been restricted to the autocorrelation in $\gamma_1(r)$ [28].

Because of the usual experimental ranges of crystallinity, the appearance of the baselines in the study of semicrystalline polymers is not very frequent [36, 37]. Therefore, the crystalline volume fraction should be obtained by other alternative techniques such as, for example, differential scanning calorimetry. In this way, if the crystallinity in volume is known, it is possible to obtain the lost baseline [37, 38]. However, if the crystallinity is either low or high, it is possible to directly obtain the baseline for which it is foreseen that the morphology is solved [36]. For example, Vonk and Pijpers and Vonk and Koga worked at high crystallinities and they observed the aforementioned baselines [39].

The presence of thermal and density fluctuations, $(I_B(q))$, causes waves in the function $\gamma_1(r)$ as reported by Defoor and Avila [40]. After extrapolating both sides of the intensity curve, the fluctuations that could not be eliminated using $(I_B(q))$ are suppressed. Also, Avila (40b) and Medellín and Avila (41) determined that the use of a two-distance sample detector when recording intensity data provides more detailed information than when data are taken with a single-distance sample detector. This is because a greater range of values of q is accessed, which allows a better estimation, particularly of $(I_B(q))$ and E.

19.5.2 Interface Distribution Function $g(r)$

A more detailed analysis of data from SAXS can be carried out by means of the interface distribution function $g_1(r)$, introduced by Ruland [30]. This function is the second derivative of the one-dimensional correlation function and is the correlation function derived from the first derivative of the local electron density function, that is,

$$g_1(r) = y_1''(r) = -\left[\rho'(r)\right]^{*2} \tag{19.50}$$

The previous function $g_1(r)$ requires the determination of the region in which Porod's law is valid in the reciprocal space. According to Ruland, since $\rho(r)$ consists of a sequence of positive and negatives steps located at the interfaces of the lamellae (Fig. 19.5), its first derivative is a series of positive and negative Dirac delta functions weighted by means of the height of the step (Fig. 19.12a) [30]. The correlation function of the first derivative consists of a series of distribution of distances with positive and negative values that correspond to the neighboring interfaces (Fig. 19.12b).

19.5.2.1 Experimental Interface Distribution Function $\mathbf{g(r)}$

When the second derivative of $\gamma_1(r)$ with respect to r is calculated for one-dimensional two-phase systems, the result is

$$\frac{\partial^2}{\partial r^2}\gamma_1(r) = -\frac{2Q}{d_P}\delta(r) + g_1(r) \tag{19.51}$$

where Q is the invariant, d_P is the average one-dimensional longitude parameter, $\delta(r)$ is the Dirac delta function at the origin, and $g_1(r)$ contains the values for $r \neq 0$. From the Fourier transform of this equation

$$q^4 I(q) = \frac{2Q}{d_P} - G_1(q) \tag{19.52}$$

where $G_1(q)$ is known as the *interference function* and is given by

$$G_1(q) = \Im\left[g_1(r)\right] = K_P - q^4 I(q) \tag{19.53}$$

From Equation 19.53, one can obtain

$$g_1(r) = \frac{t}{V}\frac{1}{2\pi^2}\int_0^\infty G_1(q)\cos(qr)\mathrm{d}q \tag{19.54}$$

where t is the thickness and V is the volume occupied by the lamellar stacks. When experimental $I(q)$ data versus q are collected in an ideal lamellar system without a finite interface, it is possible to apply this equation to obtain information about the nature of the system.

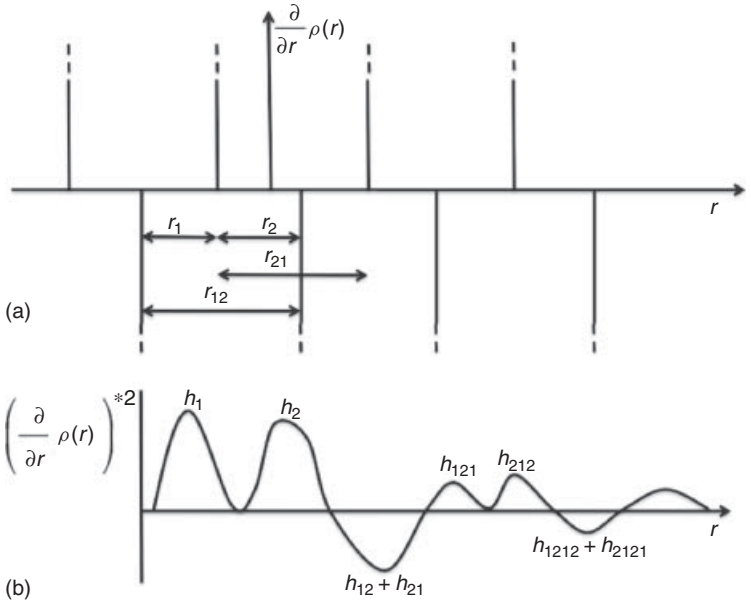

Figure 19.12 Schematic representation of (a) first derivative from $\rho(r)$ and (b) its correlation function. *Source*: Reproduced with permission from Ruland W. Colloid Polym Sci 1977;255:417 [30]. Copyright 1977 Springer.

19.5.2.2 Form and Properties of the Interface Distribution Function According to Stribeck and Ruland [42], the first distribution $h_1(r)$ of distances r_1 is positive and is related to the spacing between adjacent interfaces corresponding to the thickness of lamellae of the phase with the smaller volume concentration. The second distribution $h_2(r)$ of distances r_2 is also positive and is related to the distances between adjacent interfaces that correspond to the thickness of the lamellae of the phase with the greatest volume concentration. The following distribution $h_3(r)$ for distances r_3 is negative, and is related to the spaces of the following second interface, for example, that extending from the beginning of a region of density ρ_1 to the following region with the same density. Following the sequence, the fourth distribution $h_4(r)$ for distances r_4 will be positive and will be related to the distance of the third following interface with the lowest volume concentration and lamellae of the phase of maximum volume concentration, etc.

For the evaluation of the functions $g_1(r)$, the distributions $h_1(r)$, $h_2(r)$, $h_3(r)$, etc. should be separated from the adjacent distributions, and their statistical weights and momenta should be determined. The weights w of the distributions contain, through the weighting functions $(1 - r/t)$, the information of the size of the stacking, t. Because the signs of the weights are alternated, serious errors can be introduced when the distributions of opposite signs overlap. This effect is more severe at large distances, so that only values of w for the distributions near the origin will be significant. The same occurs with the determination of the momenta of the distributions where only the first and second momenta can be obtained with reasonable accuracy. However, an exact determination of the weights and the first and second momenta of the distributions until h_4 will allow the determination of an average value of t, and of the characteristics of the thickness of lamellae and its variation. The centers of $h_1(r)$ and $h_2(r)$ correspond to the average thicknesses l_{1m} and l_{2m} of the lamellae of density ρ_1 and ρ_2, respectively; a comparison of the variances σ_1^2 and σ_2^2 obtained from the second momenta of h_1 and h_2 with those of h_3 and h_4 can be used to study the type of statistic present in the lamellar stacking. If the distributions of the distances are overlapped even for short distances, so that an unambiguous evaluation in terms of w_i, l_i, and σ_i is difficult, then the use of theoretical models for the simulation of lamellar systems is required in order to adjust them to experimental curves.

19.5.2.3 Simulated Interface Distribution Function g(r) If Gaussian distributions are assumed to represent the variation of the interface distances, then theoretical functions $g_1(r)$ can be obtained. In this case, the function $g_1(r)$ is given by

$$g_1(r) = \sum_{i=1}^{\infty} w_i h_i \tag{19.55}$$

where w_i are the weights for the Gaussian distributions of distance h_i centered at r_i. When considering normalized

distributions, h_i is given by

$$h_i = \frac{1}{\sigma_i\sqrt{2\pi}} \exp\left[-\frac{\left(r - r_i\right)^2}{2_i^2} \right] \tag{19.56}$$

where σ_i is the standard deviation of the nth distribution of the distance. The distances r_i are given by

$$\begin{aligned} r_i &= n\left(r_1 + r_2\right) && \text{for} \quad i = 3n \\ r_i &= n\left(r_1 + r_2\right) + r_1 && \text{for} \quad i = 3n+1 \\ r_i &= n\left(r_1 + r_2\right) + r_2 && \text{for} \quad i = 3n+2 \end{aligned} \tag{19.57}$$

In these equations, n is an ascending integer that begins with 1.

For the size of infinite stacking, the weighting functions are given by

$$\begin{aligned} w_{i1} &= 1 \qquad for \quad i \neq 3n \\ w_i &= -2 \quad for \quad i = 3n \end{aligned} \tag{19.58}$$

and a first approximation for finite stacking is given by

$$\begin{aligned} w_i &= \exp\left(\frac{-r_i}{t}\right) && \text{for} \quad i \neq 3n \\ w_i &= -2\exp\left(\frac{-r_i}{t}\right) && \text{for} \quad i = 3n \end{aligned} \tag{19.59}$$

The statistics by which the phases are related depend on the theoretical model used. In general, three theoretical models are considered and these are the homogeneous lamellar model, the network model, and the lamellar stacking model. In the following paragraphs, the particular distribution relationships are presented depending on the index of the distance.

Homogeneous Lamellar Model (HLM) In this model, the variation of parameters of the lamellar structure from one stacking to another is perfectly periodic and contains the same volume fractions of the two phases. In this case σ_i/r_i are constant; for that

$$\frac{\sigma_1}{r_1} = \frac{\sigma_2}{r_2} = \frac{\sigma_3}{r_3} \ldots \sigma_i = r_i \quad \text{for every } i \tag{19.60}$$

where a single variance and two distances can be fixed in order to obtain the other related parameters.

Lattice Model (LM) This model consists of the independent variation of the thickness l_1 and the distance $L(L = r_3)$ between the centers of the lamellae of the same phase within a given stacking. The change of σ_i is given by

$$\sigma_i = n\left(\frac{\sigma_1^2}{2} + \sigma_L^2\right) \quad \text{for } i = 3n \text{ and } i = 3n \pm 1 \tag{19.61}$$

Lamellar Stacking Model (LSM) In this case, the function $g_1(r)$ results from the independent variation of the quantities σ_1 and σ_2 of the distances r_1 and r_2, respectively (equivalent to the thickness l_1 and l_2 of the lamellae of phases 1 and 2), within a given stacking. The change of σ_i is given by

$$\begin{aligned} \sigma_i^2 &= n\left(\sigma_1^2 + \sigma_2^2\right) && \text{for } i = 3n \\ \sigma_1^2 &= n\left(\sigma_1^2 + \sigma_2^2\right) + \sigma_1^2 && \text{for } i = 3n+1 \\ \sigma_1^2 &= n\left(\sigma_1^2 + \sigma_2^2\right) + \sigma_2^2 && \text{for } i = 3n+2 \end{aligned} \tag{19.62}$$

APPENDIX A PROCEDURE TO OBTAIN MORPHOLOGICAL DATA FROM 1D SAXS PROFILES

This procedure outlines the main steps used to obtain morphological data from 1D SAXS patterns of polymer samples. As an example, an isothermally crystallized sample of a copolymer containing ethylene/hexane and ethylene/butene was characterized using time-resolved synchrotron radiation at the Advanced Polymers Beamline, X27C, National Synchrotron Light Source, Brookhaven National Laboratory. The X-ray beam wavelength was 1.366 Å, and the size was circa 0.4 mm in diameter. The SAXS pattern was collected using a linear position-sensitive detector (European Molecular Biological Laboratory) with a sample-to-detector distance of 1788 mm. SAXS scattering angle was calibrated using silver behenate. Calculations were performed by the authors using Mathcad™ by the routine developed for this purpose.

19.A.1 Data Analysis

19.A.1.1 Corrections to the Experimental Data Qualitative analysis of SAXS data requires the extrapolation to both 0 and ∞ of the scattering intensity as a function of the scattering vector q. In the first case, SAXS data was extrapolated to $q \to 0$ using Debye's equation (Eq. 19.7). On the other hand, the density profile as a function of a space vector r for an ideal two-phase system resembles a squared function because the boundaries are assumed to be sharp and the density within the phases is considered as constant. In this case, Porod established that the intensity decays as the inverse of the fourth power of the scattering vector at large q values, mathematically expressed as the Porod's law, Equation 19.13. However, two-phase polymer systems often deviate from the ideality due to the presence of a density gradient between the phases as well as density variations within the phases. The latter is often associated with a background scattering I_B, which produces a positive deviation of the Porod's law, while the former corresponds to a negative deviation associated with the interface thickness

E. Assuming finite boundaries, $E = 0$, Equation 19.13 becomes

$$\underset{q\to\infty}{I(q)} = \frac{K_P}{q^4} + I_B \tag{19.A.1}$$

If enough data is acquired at large q values, K_p and I_B can be determined using nonlinear least-squares fitting and, therefore, the ideal intensity. However, the problem arises in the selection of q limits, since the choice of both the lower and upper limits significantly affects the validity of the Porod's law. In this case, the upper limit was set to $q_{upp} = 2$, and the lower limit q_{low} was varied until the minimum area of the interference function $G_1(q)$ was obtained (Eq. 19.53). Once this criterion is achieved, the interface distribution function $g_1(r)$ (Eq. 19.54) is calculated from the Fourier transform of $G_1(q)$.

19.A.1.2 Correlation Distances and Distributions The characteristic distances between each interface, as well as their statistical distributions, were obtained by means of a lamellar stacking model with infinite size to Lorentz data (I_q^2)

$$I_{ideal}(q) \bullet q^2 = \frac{K_P}{q^2} \bullet \mathrm{Re}\left[\frac{H_1 \bullet H_2}{1 - H_1 \bullet H_2}\right] \tag{19.A.2}$$

where

$$H_i = 1 - \exp\left(i \bullet r_i \bullet q - \frac{\sigma_i^2 \bullet q^2}{2}\right) \tag{19.A.3}$$

r_i corresponds to the ith interface distance, and σ_i to its corresponding standard deviation. Interface distances and their distributions were obtained by means of a nonlinear least-squares fitting of the $I_{ideal}(q) \cdot q^2$ to Equation (19.A.2). A weight factor of $1/I_{ideal}(q) \cdot q^2$ was used. The periodicity or long period L is the sum of $r_1 + r_2$. The resulting parameters are shown in Tables 19.A.1 and 19.A.2. Finally, the ideal intensity, the Lorentz intensity, the interference function, and the interface distribution function were simulated and compared with the experimental data to check for validity of the results (Figs. 19.A.1, 19.A.2, 19.A.3, and 19.A.4).

Finally, and only to show the effect of the statistics, simulations where performed using different standard deviations keeping the correlation distances shown in

TABLE 19.A.1 Experimental Parameters Obtained in Reciprocal-Space Analysis

$q \to 0$		$q \to \infty$			Whole Range	
A	e	K_P	E (nm)	I_B	Q	Area $G_1(q)$
1280	7.91	18.676	0.000	5.709	36.41	0.343

TABLE 19.A.2 Experimental Parameters Obtained in Real-Space Analysis

Correlation Distance (nm)			Standard Deviation (nm)		
r_1	r_2	L	s_1	s_2	s_L
6.59	2.06	8.64	2.731	1.472	3.102

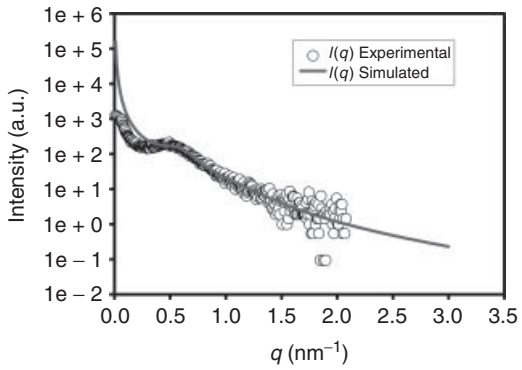

Figure 19.A.1 Intensity plot. (*See insert for the color representation of the figure*.)

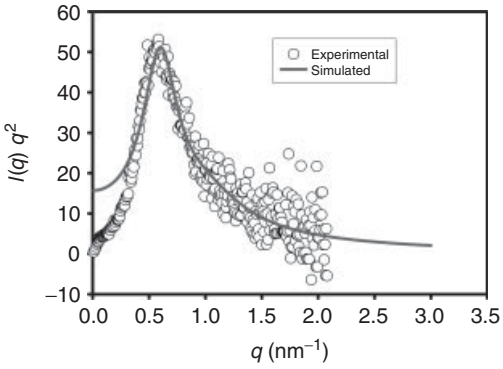

Figure 19.A.2 The Lorentz plot. (*See insert for the color representation of the figure*.)

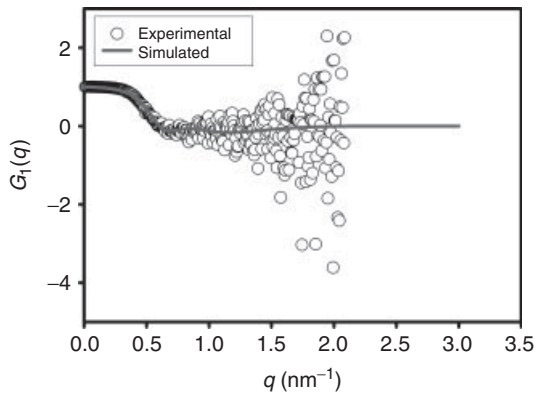

Figure 19.A.3 Interference function. (*See insert for the color representation of the figure*.)

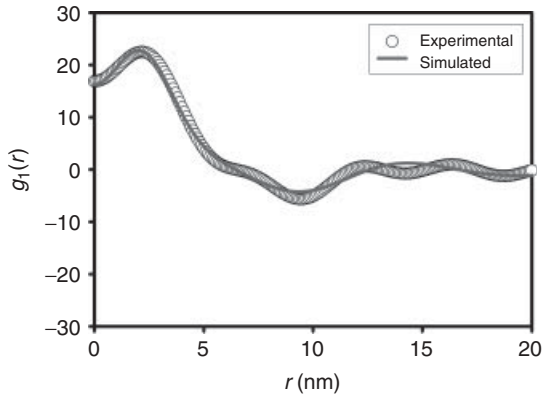

Figure 19.A.4 Interface distribution function. (*See insert for the color representation of the figure*.)

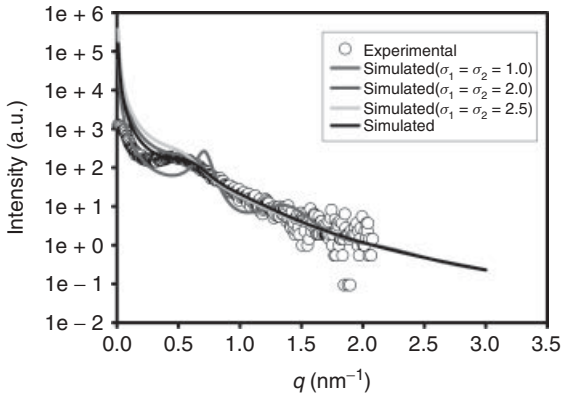

Figure 19.A.5 Statistical effect on the intensity plot. (*See insert for the color representation of the figure*.)

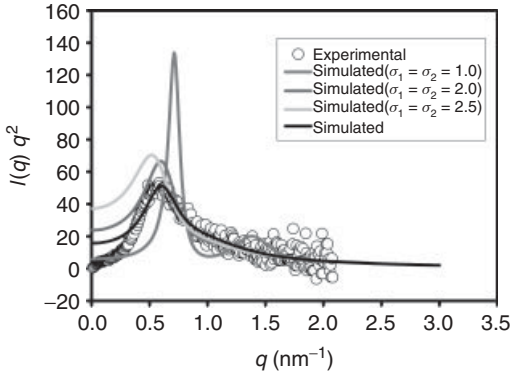

Figure 19.A.6 Statistical effect on the Lorentz plot. (*See insert for the color representation of the figure*.)

Table 19.A.2. The results are presented in Figures 19.A.5, 19.A.6, 19.A.7, and 19.A.8. These results indicate that the statistical variation in the distances can have a profound effect in the shape of the different functions in both reciprocal and real space.

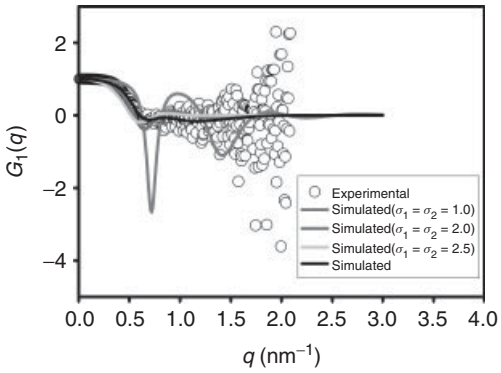

Figure 19.A.7 Statistical effect on the interference function. (*See insert for the color representation of the figure*.)

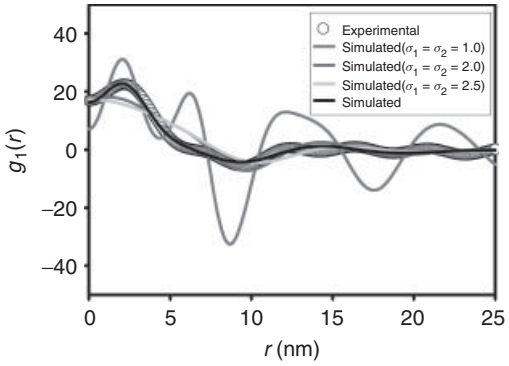

Figure 19.A.8 Statistical effect on the interface distribution function. (*See insert for the color representation of the figure*.)

REFERENCES

1. Sperling LH. *Introduction to Physical Polymer Science*. Hoboken: John Wiley and Sons; 1999. p 845.
2. Bassett DC. *Principles of Polymer Morphology*. Cambridge: Cambridge University Press; 1981. p 251.
3. Schultz J. *Polymer Materials Science*. Upper Saddle River: Prentice-Hall; 1974. p 524.
4. [a] Fischer EW, Z. Z. Naturforsch. 1957, 12a, 753; [b] Keller A. Philos Mag 1957;2:1171–1175. [c] Till PH. J Polym Sci 1957;24:301.
5. Keith HD, Padder FJ. J Appl Phys 1963;34:2409.
6. [a] Bunn CW, Alcock TC. Trans Faraday Soc 1945;41:317. [b] Keller A. J PolymSci 1955;17:291.
7. [a] Mitsuhashi S. Bull Text Res Inst 1963;66:1. [b] Pennings AJ, Kiel AM. Kolloid Z Z Polym 1965;205:160–162. [c] Binsbergen FL. Nature 1966;211:516.
8. Hoffman JD, Davis GT, Lauritzen JI. The rate of crystallization of linear polymers with chain folding. In: Hannay NB, editor. *Treatise Solid State Chemistry*. Volume 3. New York: Plenum Press; 1976. p 418508, 520.

9. Alexander LE. *X-Ray Diffraction Methods in Polymer Science*. New York: Wiley Interscience; 1969. p 582.
10. Porod G. *General Theory in: Small-angle X-ray Scattering*. London: Academic Press; 1982. p 515.
11. Ruland W. J Appl Crystallogr 1971;4:70.
12. Debye P. Ann Phys 1915;351:809.
13. [a] Guinier A, Fournet G. *Small Scattering of X-Rays*. New York: Wiley; 1955. p 268. [b] Debye P, Anderson HR, Brumberger H. J Appl Phys 1957;28:679.
14. Crist B. J Polym Sci Polym Phys Ed 1973;11:635.
15. Bragg WL. Camb Philos Soc 1913;17:43.
16. [a] Geil PH. *Polymer Single Crystal*. Rockland: Interscience; 1962. [b] Fischer EW, Goddar H, Schmidt GF. Kolloid Z Z Polym 1968;226:30. [c] Davis HA, VanVeld RD, Billica HR. Bull Am Phys Soc 1971;16. [d] McHugh AJ, Schultz JM. Philos Mag 1971;24:155. [e] Bassett DC, Phillips JM. Polymer 1971;12:730. [f] Statton WO. J Polym Sci 1959;41:143.
17. Baltá-Calleja FJ, Vonk CG. *X-ray Scattering of Synthetic Polymers*. Amsterdam: Elsevier; 1989. p 317.
18. Geil PH. *Small-angle Scattering from Fibrous and Partially Oriented Systems*. New York: Intersience; 1966. p 149.
19. Brundell DJ. Polymer 1978;19:1258.
20. Vonk CG, Kortleve G. Kolloid Z Z Polym 1967;220:19.
21. [a] Blundell DJ. Acta Crystallogr Sect A: Found Crystallogr 1970;26:476. [b] Blundell DJ. Acta Crystallogr Sect A: Found Crystallogr 1970;26:472.
22. Crist B, Morosoff N. J Polym Sci Polym Phys Ed 1973;11:1023.
23. Atkins EDT. *Comprehensive Polymer Science*. New York: Pergamon; 1989.
24. [a] Porod G. Kolloid-Z 1951;124:83–114. [b] Porod G. Kolloid-Z 1952;125:51.
25. [a] Tsvankin DY. Vysokomol Soyed 2078;1964:11. [b] Tsvankin DY. Vysokomol Soyed 2083;1964:11.
26. Siemann U, Ruland W. Colloid Polym Sci 1982;260:999.
27. Koberstein JT, Morra B, Stein RS. J Appl Crystallogr 1980;13:34.
28. Vonk CG. J Appl Crystallogr 1973;6:81.
29. [a] Rathje J, Ruland W. Colloid Polym Sci 1976;254:358. [b] Wiegand W, Ruland W. Colloid Polym Sci 1979; 66:355.
30. Ruland W. Colloid Polym Sci 1977;255:417.
31. Bornschlegl E, Bonart R. Colloid Polym Sci 1980;258:319.
32. [a] Medellín-Rodríguez FJ, Avila-Orta CA. Av Ing Quimica 1996;6(2):152. [b] Medellín-Rodríguez FJ, Avila-Orta CA. Av Ing Quimica 1996;6(2):156.
33. Debye P, Bueche AM. J Appl Phys 1949;20:518.
34. Chalkley HW, Cornfield J, Park H. Science 1949;110: 295.
35. Fulcher KU, Brown DS, Wetton RE. J Polymer Sci C 1972;38:315.
36. Strobl GR, Schneider M. J Polym Sci Polym Phys Ed 1980;18:1343.
37. Strobl GR, Schneider MJ, Voigt-Martin IG. J Polym Sci Polym Phys Ed 1980;18:1361.
38. Medellin-Rodriguez FJ, Phillips PJ, Lin JS. Macromolecules 1995;28:7744.
39. [a] Vonk CG, Pijpers AP. J Polym Sci Polym Phys Ed 1985;23:2517. [b] Vonk CG, Koga Y. J Polym Sci Polym Phys Ed 1985;23:2539.
40. [a] Defoor F. Molecular, Thermal and Morphological Characterization of Narrowly Branched Fractions of 1-Octene LLDPE, Ph.D. Thesis, Katholieke Universiteit Leuven, Belgium 1992; [b] Avila-Orta CA. Contribución al estudio de la morfología de polímeros semicristalinos a través de dispersión de rayos-X en ángulos bajos, BSc Thesis, Universidad Autonoma de San Luis Potosí, Mexico 1994.
41. Medellín-Rodríguez FJ, Avila-Orta CA. Av Ing Quimica 1995;5(2):191.
42. Stribeck N, Ruland W. J Appl Crystallogr 1978;11:535.